Article

Harnessing Chitosan Beads as an Immobilization Matrix for nZVI for the Treatment of Cr(VI) Contaminated Laboratory Residue

Ignacio Daniel Rychluk , Ulises Casado , Víctor Nahuel Montesinos * , Natalia Quici *

Posted Date: 11 September 2024

doi: 10.20944/preprints202409.0850.v1

Keywords: nanocomposites; chitosan; nZVI; hexavalent chromium; laboratory residue

Article

Harnessing Chitosan Beads as an Immobilization Matrix for nZVI for the Treatment of Cr(VI) Contaminated Laboratory Residue

Ignacio Daniel Rychluk [1,2], Ulises Casado [3], Víctor Nahuel Montesinos [2,4,*] and Natalia Quici [2,4,*]

[1] Instituto Sabato, CNEA. Universidad Nacional de San Martin, Gral. Paz 1499, San Martín, Buenos Aires, Argentina
[2] División Química de la Remediación Ambiental, Centro Atómico Constituyentes, CNEA-CONICET, Gral. Paz 1499, San Martín, Buenos Aires, Argentina
[3] Instituto de Investigaciones en Ciencia y Tecnología de Materiales (INTEMA), CONICET, Colon 10850, Mar del Plata, Argentina
[4] Centro de Tecnologías Químicas, Departamento de Ingeniería Química, FRBA-UTN, Medrano 951, CABA, Argentina
* Correspondence: vnmontesinos@gmail.com (V.N.M.); natalia.quici@gmail.com (N.Q.)

Abstract: Nanocomposites (NCs) consisting of zero-valent iron nanoparticles (nZVI) immobilized in chitosan (CS) were prepared and employed, for the removal of hexavalent chromium (Cr(VI)) from both synthetic and real wastewater. Medium (MCS) and high (HCS) molecular weight chitosan and stabilization with carboxymethylcellulose (CMC), and different nZVI load were explored. Characterization through Scanning Electron Microscopy with Energy Dispersive X-ray Analysis (SEM-EDS) and X-ray Diffraction (XRD) revealed millimeter-sized spheres with micrometer-sized nZVI clusters randomly distributed. Better nanoparticle dispersion was observed in NCs from the CMC-MCS and HCS combinations. Fourier-transform infrared spectroscopy (FTIR) analysis indicated that CS binds to Fe(II) or Fe(III) on the surface of nZVI through its functional groups -CONH-, -N-H and -C-OH and through the $-COO^-$ functional group of CMC, forming a bidentate bridge complex. Through experiments with synthetic waters, it was found that the elimination of Cr(VI) is favored by lowering the pH, obtaining the maximum percentage of Cr(VI) removal at pH 5.5. With real waters, it was shown that increasing the mass of NCs also improves the removal of Cr(VI), following a pseudo-second-order adsorption kinetics. The synthesized materials show great potential for applications in environmental remediation, showing good efficiency in the removal of Cr(VI) in wastewater.

Keywords: nanocomposites; chitosan; nZVI; hexavalent chromium; laboratory residue.

1. Introduction

Managing hazardous wastes within institutions engaged in education and research, presents a pressing challenge. The heterogeneity of the waste stream, which can include highly toxic compounds in a wide variety of aqueous matrixes, adds complexity to the management process [1]. Maintaining optimal working conditions necessitates proper control and management of these wastes, which is a fundamental aspect of any laboratory [2]. Although the volume of waste generated may be relatively lower than that of industrial settings, these institutions often resort to outsourcing waste management services rather than developing internal treatment solutions. These third-party services for waste treatment can translate in a financial burden. According to Antoniassi et. al. [3], the operating costs for outsourcing the collection and treatment of waste from university laboratories in Brazil can reach up to USD 1.33 per liter. This amounts to approximately USD 251.28 per month and USD 3,015.42 annually. In Argentina, at the National Atomic Energy Commission (CNEA), the

 doi:10.20944/preprints202409.0850.v1

reported cost for treating 1 kg of liquid waste contaminated with Cr(VI) is 0.64 USD, excluding shipping expenses, as disclosed by the company IDM S.A (April 2024).

As an illustrative case, the Liquid Effluents Laboratory of the National Institute of Industrial Technology in Argentina (INTI) annually produces 30 liters of liquid waste contaminated with Cr(VI). This effluent primarily comprises $K_2Cr_2O_7$ standard solutions and dilutions resulting from water quality determinations conducted in accordance with IRAM 29111:2006 and IRAM 29130:2004 standards. Historically, this waste stream has been managed by an external waste management company. However, establishing the capability to treat the wastewater internally within the laboratory is becoming increasingly pertinent. Laboratory staff typically possess the technical knowledge to operate a water treatment reactor or implement a water treatment protocol, making this transition feasible. Such autonomy from external providers not only ensures independence but also facilitates the potential recycling of water utilized in water quality assessments. An alternative to treat this type of effluent is to use remediation technologies that reduce the volume generated, which facilitates its treatment or subsequent management. Iron-based nanomaterials, particularly zero-valent iron nanoparticles (nZVI), have gained widespread use in environmental remediation, emerging as promising alternatives in pollutant removal processes, attributed to their inherent redox reactivity [4–6] targeting the removal of various contaminants such as nitro aromatics, dyes, heavy metals, and chlorinated compounds [7–9] thus showcasing their versatility and applicability across diverse environmental cleanup scenarios.

The mechanisms for removing aqueous Cr(VI) using zero-valent iron nanoparticles are well established. The chemical reactions involved can be described as follows [10]

$$2HCrO_4^- + 3Fe^0 + 14H^+ \rightarrow 3\,Fe^{2+} + 2Cr^{3+} + 8H_2O \quad (1)$$

$$2CrO_4^{2-} + 3Fe^0 + 16H^+ \rightarrow 3\,Fe^{2+} + 2Cr^{3+} + 8H_2O \quad (2)$$

$$HCrO_4^- + 3Fe^{2+}_{sol/\,sup.} + 7H^+ \rightarrow 3Fe^{3+}_{sol/\,sup.} + Cr^{3+} + 4H_2O \quad (3)$$

$$CrO_4^{2-} + 3Fe^{2+}_{sol/\,sup.} + 8H^+ \rightarrow 3Fe^{3+}_{sol/\,sup.} + Cr^{3+} + 4H_2O \quad (4)$$

The use of nZVI for the removal of Cr(VI) enables compliance with the regulations of maximum concentrations allowed in liquid waste discharges, as established by organizations such as the World Health Organization (WHO), the California Environmental Protection Agency (CALEPA) and the Matanza-Riachuelo Basin Authority in Argentina (known in Spanish as ACUMAR). The WHO sets a limit of 50 $\mu g\ L^{-1}$ for Cr(VI), while CALEPA has set even lower levels. According to ACUMAR [11], the discharge limit in liquid effluents should be $\leq 0.2\ mg\ L^{-1}$ for Cr(VI) and $\leq 2\ mg\ L^{-1}$ for total chromium (Cr(TOTAL)).

Despite the efficacy of nZVI as removal agents, the potential leaching of post-removal iron may be a limitation for the wider application of nZVI based processes, as the environmental fate of nZVI nanoparticles remains unclear [12]. In addition, nZVI nanoparticles tend to agglomerate in aqueous media, resulting in a loss of surface area, reactivity, and mobility [13]. An alternative to overcome these drawbacks is the immobilization of nZVI forming millimeter sized nanocomposites (NCs). These NCs have the potential to be employed in continuous flow systems, filling columns, or acting as reactive barriers. In the past decade, several studies have highlighted the effectiveness of immobilizing nZVI for removing contaminants like chromium [6].

Polymer matrices, such as chitosan (CS), have gained relevance in immobilizing iron nanoparticles for environmental applications [14–16]. CS comes from chitin, the second most common biopolymer in nature after cellulose. The industrial production of CS uses chemical and biological methods that deacetylate chitin, generating variants with different molecular weights and degrees of deacetylation [17]. These variations can influence the structural properties of the CS, affecting the stability and strength of the resulting NCs. Selecting CSs with specific molecular weights can prevent these problems. In this work, documented synthesis procedures were followed, using CSs of different molecular weights to compare the mechanical stability of the materials obtained.

The presented work focuses on the effective immobilization nZVI within a CS polymeric matrix, with special attention to its ability to efficiently remove Cr(VI) from wastewater. The goal is to design

 doi:10.20944/preprints202409.0850.v1

an accessible, efficient treatment method that enables the reuse of wastewater from analyses related to water quality in laboratory settings. To optimize the synthesis, various routes were tested, including the pre-stabilization of the nZVI with CMC and the exploration of different molecular weights of chitosan, resulting in NCS with improved mechanical stability and reactivity. The materials produced were thoroughly characterized using multiple techniques, confirming their structure and stability. The practical relevance of this work is highlighted by the ability of the NCs to meet water quality regulations while also offering a cost-effective solution for the treatment of Cr(VI)-contaminated wastewater.

2. Materials and Methods

2.1. Materials and Chemicals

nZVI (NANO STAR, hereinafter NSTAR) were supplied by NANO IRON, s.r.o. (Czech Republic) with a Fe(0) ≥ 65-80%. Its composition information is included in the supporting information file. Chitosan powder of medium and high molecular weight (MCS and HCS, respectively) and sodium carboxymethylcellulose (CMC, molecular weight ~ 250000) were provided by Sigma Aldrich. Synthetic Cr(VI) containing water was prepared using $K_2Cr_2O_7$ provided by Merck. Glacial acetic acid (CH_3COOH) 99-100%, hydroquinone and 1,5-diphenylcarbonazide were provided by Merck. NaOH, triethanolamine (TEA), H_2SO_4 and phosphoric acid, were all analytical grade or higher and provided by Biopack. o-phenanthroline was from Mallinckrodt and N_2 (≥ 4.8) was provided by Linde. milli-Q water (resistivity = 18 MΩ cm^{-1}) was utilized in all syntheses. The Cr(VI) containing effluent was provided by the Liquid Effluents Laboratory of INTI and its main compositional characteristics are summarized in Table 1.

Table 1. pH, TOC and elemental composition of the laboratory Cr(VI) contaminated effluent.

Sample type	pH	TOC (ppm)	Composition	Concentration (ppm)
Aqueous	6.5	TC: 3.77 IC: 3.55 TOC: 0.22	S	12.08 ± 0.16
			Cl	64.18 ± 0.31
			K	26.98 ± 0.13
			Ca	76.96 ± 0.18
			Cr	31.94 ± 0.073
			Fe	0.055 ± 0.002
			Zn	0.03 ± 0.001

TC: Total Cabon, TOC: Total Organic Carbon and IC: Inorganic Carbon.

2.2. Synthesis of NCs

The work of Cumbal et al. [18] was used as a starting point for the NCs synthesis. In brief, an acidified suspension of NSTAR containing dissolved CS was gradually added dropwise to a NaOH solution to induce the coagulation of the droplets. To prepare the suspension, 0.478 g NSTAR were added to 50 mL of a 20 g L^{-1} CS solution in acetic acid 2% v/v under continuous N_2 bubbling to ensure anoxic conditions. Subsequently, the suspension was dripped using a syringe pump at a rate of 50 µL s^{-1} into 500 mL of a 0.5 M NaOH solution, which had been previously purged with N_2. In cases where CMC stabilization of nZVI was used, the NSTAR were previously suspended in 5 mL of aqueous CMC 4 g L^{-1} solution by applying ultrasound for 15 min. Spheres obtained (NCs) were kept for 24 h in NaOH to harden and, finally, they were washed and preserved in deoxygenated milliQ water until use.

Hereafter, the NCs will be referred as NSTAR@MCS or NSTAR@HCS, depending on the type of CS used in the synthesis. In cases where CMC was added, the names will be NSTAR-CMC@MCS or NSTAR-CMC@HCS.

All NCs had an Fe(0) mass content of 24%, except for NSTAR@MCS, which had an Fe(0) content of 6%. In addition, beads containing only the different polymer matrices used (HCS, CMC@MCS, and CMC@HCS) were synthesized to understand their role in the Cr(VI) removal.

 doi:10.20944/preprints202409.0850.v1

2.3. Characterization of NCs

The synthesized NCs were characterized by X-ray diffraction (XRD), scanning electron microscopy with energy-dispersive microanalysis (SEM-EDS) and Fourier transform infrared spectroscopy (FTIR). In all cases, the NCs were first dried in a desiccant vessel containing silica gel under vacuum.

XRD measurements were performed over dried and physically ground NCs. The powder samples were analyzed with a PanAnalitycal Empyrean diffractometer equipped with a PIXcel 3D detector, employing Cu-Kα radiation (λ = 1.542 Å). The 2θ range varied between 10 and 90°, with a step of 0.026° and 24 seconds of counting per step.

SEM analysis was conducted in a Phillips Quanta 200 scanning microscope with voltage 20 kV. X-ray energy dispersion spectrometry (EDS) measurements were performed with an EDAX Apollo detector. To enhance image contrast, the spheres were metallized with Au using a spray coating evaporator (Quorum model Q150T ES) and mounted on conductive carbon biface tape. In selected samples of NCs, elemental distribution analysis of C, O and Fe was conducted using SEM-EDS mapping. The same mapped regions were further characterized using secondary electrons (SE).

Compression tests were performed by Dynamic Mechanical Analysis (DMA) using a Perkin Elmer DMA 7e equipment with parallel plate geometry of 10 mm at 20 °C, where a force in the range of 1 to 400 mN min^{-1} was applied to evaluate the Stress vs. Strain (%) achieved by the tested material. Due to the low compressive strength of the synthesized materials, tests were carried out by placing 3 spheres of the same material simultaneously in contact with each other. DMA testing was only performed on the NCs with Cr(VI) removal potential, i.e., the NCs that showed mechanical robustness. Both the experimental arrangement and the procedure used are described in the supporting information.

FTIR-ATR measurements were carried out with a NICOLET 560 spectrometer equipped with an MCT-A detector cooled with liquid N_2. A horizontal ZnSe-ATR single reflection unit (area = 615 mm^2) was employed to detect the surface interactions between polymers and NSTAR. The measurement protocol was based in the one reported by Weisz et. al. [19]. Initially, spectra of CS and CMC aqueous solutions were acquired by depositing a drop containing 20 g L^{-1} of each polymer onto the ATR crystal. Subsequently, serial dilutions were performed to determine the concentration at which no signal was detected, referred to as CS-0 or CMC-0, respectively. Next, the ATR glass was then partially coated with a concentrated suspension of NSTAR to form a film, which was left to air dry for 24 h. A drop of CS-0 or CMC-0 was applied to the NSTAR film, and then the IR spectra were reacquired.

2.4. Removal of Cr(VI)

The capacity of the synthesized NCs to remove Cr(VI) from an aqueous solution was investigated through batch experiments. Solutions of Cr(VI) with a concentration of 65 µM were prepared, and the pH was adjusted to a range of 3 to 11 using 0.5 N H_2SO_4 or 0.5 M NaOH. The solutions were placed in tubes containing 25 mL of the Cr(VI) solution and 0.7 g of NCs, and maintained under orbital agitation for 2 h.

In the case of the Cr(VI) containing effluent, removal experiments were conducted by adding 1 to 6 g of NSTAR@HCS to 50 mL of effluent. The pH of the NCs was adjusted to 6.5, equal to that of the effluent and the mixture was left in contact for 24 hours.

In all cases, samples were withdrawn to determine the concentration of Cr(VI) using the diphenylcarbazide (DFZ) method [20] with a UV-Vis Hewlett Packard Agilent 8453 spectrophotometer. The determination of the total chromium concentration (Cr(TOTAL)) was done by total X-ray reflection fluorescence (TXRF) using Ga as an internal standard (10 µL aliquot of a 100 mg L^{-1} Ga solution to 990 µL of each sample). Subsequently, 10 µL of the resulting solutions were deposited onto a quartz disc and inserted into a S2 PICOFOX (Bruker) spectrometer for measurement.

Samples were analyzed to determine Total Organic Carbon (TOC) using a Total Organic Carbon and Total Nitrogen Analyzer (TOC/TN) (Shimadzu TOC-L/TNM-L) after 24 hours.

 doi:10.20944/preprints202409.0850.v1

2.5. Cr(VI) Removal Capacity Using NCs

The dry-based (DB) Cr(VI) removal capacity of the NCs (q_t^{DB}, mg Cr(VI) $g^{-1}_{NC_{DB}}$) was calculated using Eq. (5).

$$q_t^{DB} = \frac{\%R^{Cr(VI)} \times [Cr(VI)]_0 \times V^{effluent} \times M_r^{Cr}}{m(nZVI+CS)_{DB}} \quad (5)$$

Where $\%R^{Cr(VI)}$ represents the percentage of Cr(VI) removal obtained in the experiments calculated as $(1-[Cr(VI)]_t/[Cr(VI)]_0)\times 100$, $[Cr(VI)]_0$ is the initial concentration of Cr(VI) in the effluent (mM), $V^{effluent}$ is the volume of the effluent, M_r^{Cr} is the molar mass of Cr (52 g mol^{-1}), and $m(nZVI+CS)_{DB}$ represents the total dry-based solid mass of the material used. This value was obtained by drying the material and corresponds to the 3% of the NCs weighed in each experiment.

2.6. Kinetic Fittings

The results obtained from the Cr(VI) removal experiments over time were analyzed using the pseudo-first order (Eq. (6)), pseudo-second order (Eq. (7)) [21], and intraparticle diffusion (Eq. (8)) [15] models.

$$\ln\left(1-\frac{q_t^{WB}}{q_e^{WB}}\right) = -k_1 \times t \quad (6)$$

$$\frac{t}{q_t^{WB}} = \frac{1}{k_2 \times (q_e^{WB})^2} + \frac{1}{q_e^{WB}} t \quad (7)$$

$$q_t^{WB} = k \times \sqrt{t} \quad (8)$$

Where q_e^{WB} is the wet-based (WB) equilibrium removal capacity ($mg\ g^{-1}$), q_t^{WB} is the WB adsorption at time "t" (mg g^{-1}), k_1 (min^{-1}) y k_2 (g mg^{-1} min^{-1}) are the rate constants of pseudo-first order and pseudo-second order kinetics, respectively, and k (mg g^{-1} $min^{1/2}$) is the intraparticle diffusion constant.

3. Results and Discussion

3.1. Synthesis and Characterization of Synthesized Materials

3.1.1. Structure of the NCs

NCs exhibit a spherical morphology and are millimeter-sized, with an average diameter of 2 ± 0.5 mm. NSTAR-CMC@MCS, NSTAR@HCS and NSTAR-CMC@HCS display a black coloration due to the presence of nZVI. In contrast, NCs prepared solely with MCS (NSTAR@MCS) exhibit a reddish-brown hue, possibly indicating nZVI oxidation.

3.1.2. XRD

Figure 1 shows the XRD spectra obtained for NSTAR@MCS, NSTAR-CMC@MCS, NSTAR@HCS, NSTAR-CMC@HCS and free NSTAR. It can be observed that all the NCs studied and the free NSTAR exhibit a dominant phase of α-Fe, except for those synthesized solely from MCS. Consequently, NSTAR@MCS was ruled out as a material for Cr(VI) removal.

 doi:10.20944/preprints202409.0850.v1

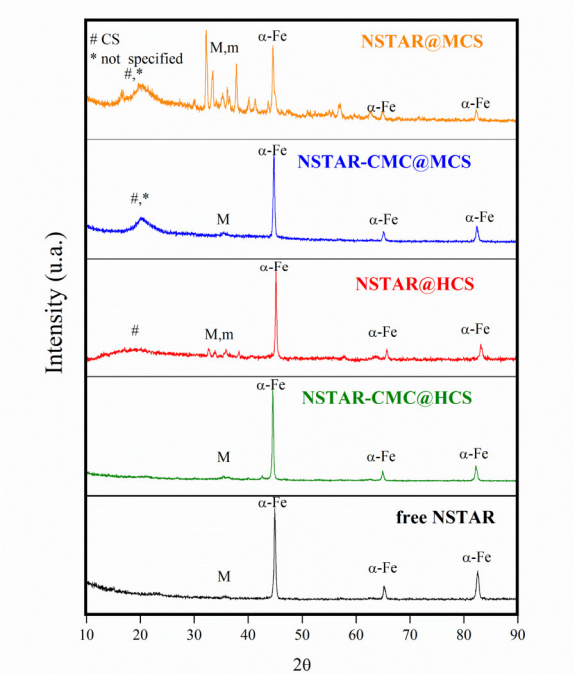

Figure 1. Diffraction spectra of NSTAR@MCS, NSTAR-CMC@MCS, NSTAR@HCS, NSTAR-CMC@HCS and free NSTAR. The peaks identified as #, M, m and * correspond to CS, magnetite, maghemite and an unidentified substrate, respectively.

The main peaks of α-Fe are observed at 45°, 65°, and 82°, along with a set of low-intensity peaks below 35° that typically correspond to magnetite or maghemite phases. This technique cannot distinguish whether the peak at 35° corresponds to magnetite or maghemite, as both phases have the same type of crystal structure (inverse spinel) [22]. Additionally, a broad peak at 20° was observed, attributed to chitosan [23], along with peaks at 13° and 16° that could not be assigned. In the case of NCs synthesized from MCS, spectra of the NCs where CMC was added showed α-Fe at 45° as the dominant phase, while spectra of the NCs without CMC exhibited strong signals of iron oxides. This suggests that using CMC as a stabilizer prevents nZVI oxidation. When only HCS was used in the synthesis, the spectra showed iron oxides signals similar in magnitude to those observed for free NSTAR. NSTAR-CMC@HCS, however, exhibited a diffractogram most similar to free NSTAR, with minimal contribution from oxidized phases.

This preservation of the α-Fe phase when using HCS correlates with a protective effect due to a higher polymerization degree compared to MCS. The degree of polymerization, which represents the length of the polymer chains, correlates directly with the average molecular weight (Mn). Increasing both the degree of polymerization and Mn enhances the polymer's mechanical stress tolerance [17] but also prevents nZVI from oxidation. During synthesis, NSTAR are exposed to an acidic environment that favors its oxidation. HCS provides greater resistance to the acid treatment, thereby preventing NSTAR oxidation during the initial synthesis stage. A similar protective effect was observed with the addition of CMC during synthesis. The longer chain structure of HCS makes it less soluble in water, leading to greater steric hindrance around the NSTARs. This hindrance inhibits NSTAR oxidation by dissolved oxygen under acidic conditions.

3.1.3. SEM-EDS

Figure 2 shows the SEM images obtained using secondary electrons (SE) collection and the distribution of C, Fe and O for the synthesized NCs. NSTAR-CMC@MCS and NSTAR@HCS samples exhibit a well-dispersed brightness throughout their structure, indicating an increased distribution of NSTAR within the nanocomposite compared to NSTAR@MCS. On the other hand, compared with those synthesized from MCS and CMC-MCS, NSTAR@HCS were more resistant to drying and metallization processes necessary for SEM evaluation, as they maintained a spheroidal structure like

 doi:10.20944/preprints202409.0850.v1

that observed for the hydrated spheres. NSTAR@HCS maintained its spherical structure, likely due to the higher resistance provided by the longer chain structure of HCS. This resistance was also evident in the preservation of the structure during washing and agitation.

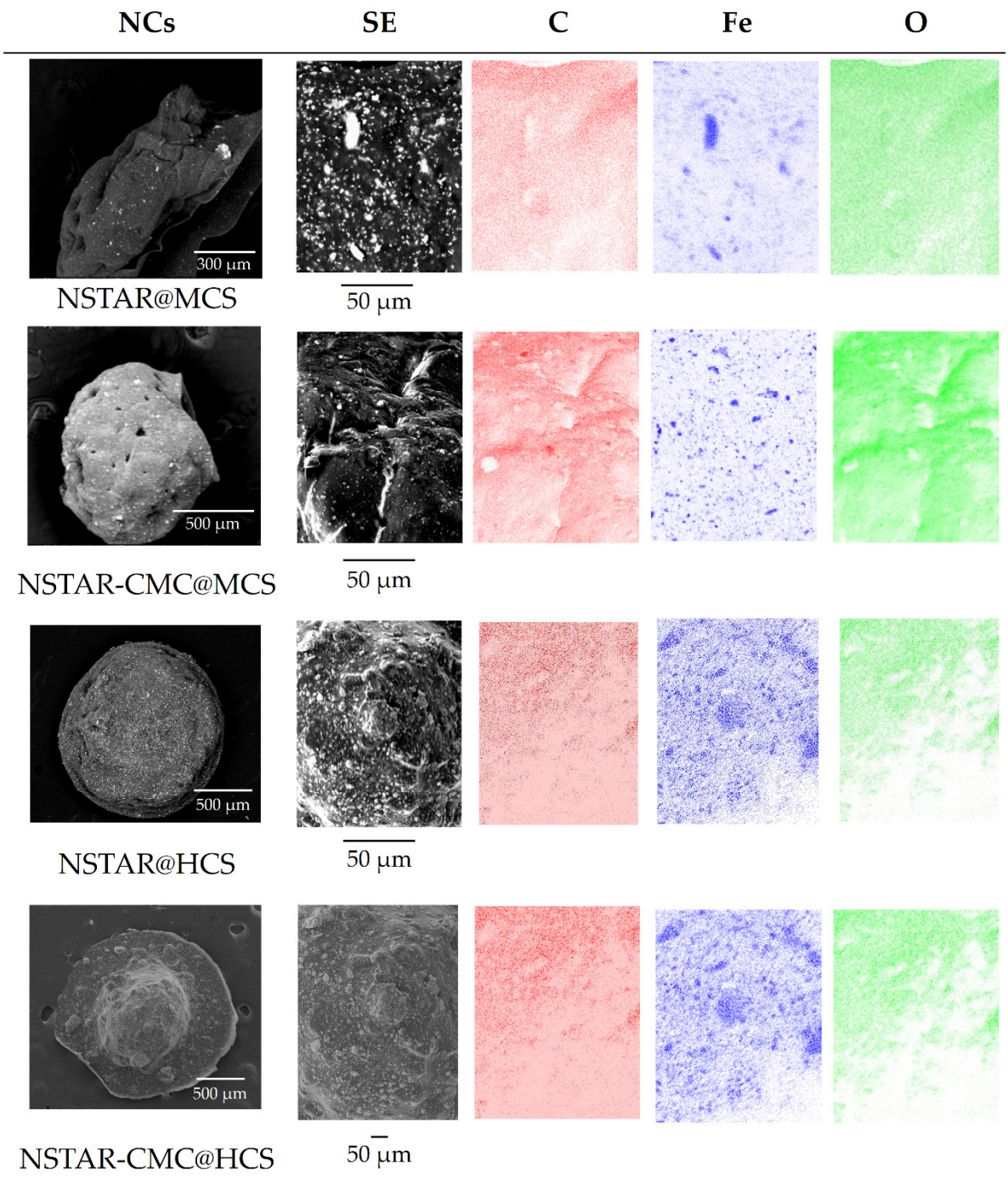

Figure 2. SEM images of secondary electrons (SE) for the samples: NSTAR@MCS, NSTAR-CMC@MCS, NSTAR@HCS and NSTAR-CMC@HCS, including the distribution of C, Fe and O.

While oxygen mapping does not provide relevant information, as it can be present both the polymeric matrix and on the nZVI surface as oxide anion, C distribution resulted in the negative image of Fe mapping, in good agreement with the distribution of bright areas in the SE images. In the case of NSTAR-CMC@MCS, it was observed that some bright spots in the SE image simply corresponded to areas closer to the detector focus.

 doi:10.20944/preprints202409.0850.v1

3.1.4. Dynamic Mechanical Analysis

Figure 3 shows the stress*-strain curves, along with the compression modulus (M) fit obtained from the DMA for NSTAR@HCS (Figure 3.a), NSTAR-CMC@HCS (Figure 3.b), HCS (Figure 3.c), NSTAR-CMC@MCS (Figure 3.d) and beads. The comparison of the curves is included in the supporting information.

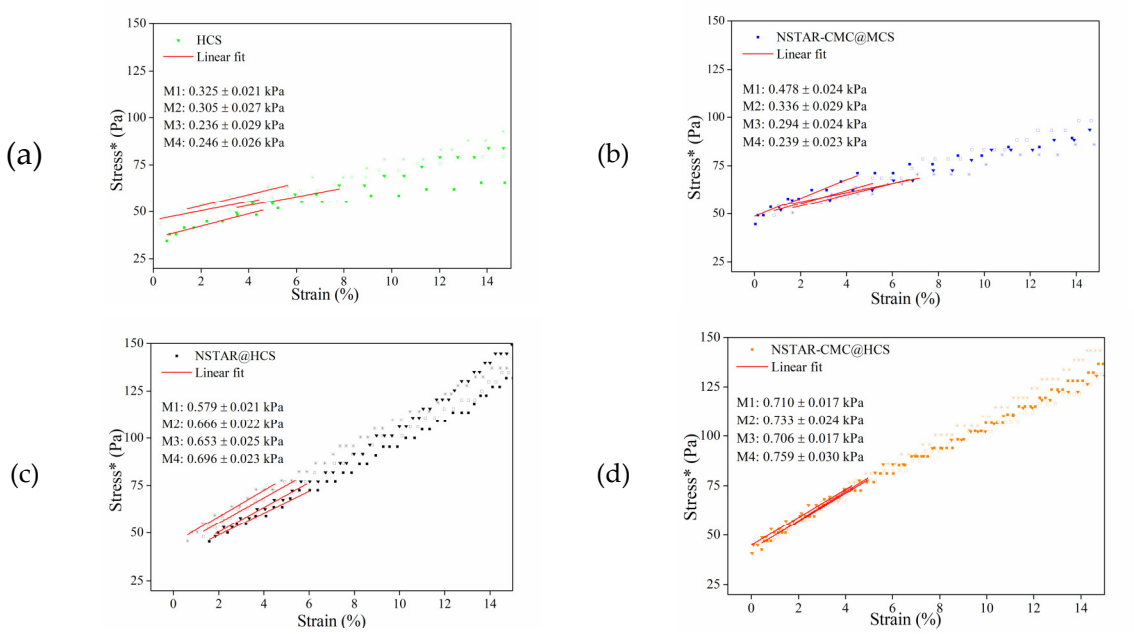

Figure 3. Stress*-strain and M curves obtained from the DMA for (a) HCS, (b) NSTAR-CMC@MCS, (c) NSTAR@HCS, and (d) NSTAR-CMC@HCS.

Defining M as the slope of the stress*-strain curve until reaching 4% strain from the beginning of the test, it is observed that according to the average values of M, we can order the samples from higher to lower mechanical resistance as follows: NSTAR-CMC@HCS (0.727 ± 0.022 kPa) > NSTAR@HCS (0.648 ± 0.023 kPa) > NSTAR-CMC@MCS (0.337 ± 0.025 kPa) > HCS (0.277 ± 0.026 kPa). Based on these M values, the following observations can be made: (1) incorporating NSTAR into an HCS matrix increases the mechanical strength of the NCs; (2) adding CMC during the synthesis slightly enhances their mechanical resistance; and (3) using HCS provides greater resistance compared with MCS.

The third finding is consistent with the increase in Mn and the degree of polymerization, since longer chains have higher intermolecular forces, which hinders their sliding and provides a greater transfer of stresses [24]. On the other hand, the slight increase in resistance provided by CMC incorporation does not justify the added synthesis step and associated costs. Therefore, using HCS as the sole polymer was determined to be the best option among all the alternatives explored.

It should be noted that the M values obtained for all the tested materials are relatively low, but in the range reported for chitosan hydrogels (0.5–1.5 kPa) [25,26] and comparable to those of healthy biological tissues (0.1–1 kPa) [27]. An alternative to improve the mechanical strength of NCs could involve the use of crosslinkers such as glutaraldehyde (GLA) [28] or tripolyphosphate (TPP) [29], although they were not explored in this study.

3.1.5. FTIR-ATR

The FTIR spectra for pure CS and CMC used in this work (Figure 4 (a) and (b)) shows typical bands of their main functional groups: -CONH- (amide C=O stretching, 1712 cm^{-1}), $-NH_2$ (NH_2 bending, 1632 cm^{-1}), -C-N (C-N stretching, 1548 cm^{-1}), $-CH_2$ (CH_2 bending 1412 cm^{-1}), -C-O-C (C-O-C stretching, 1149 cm^{-1}) -N-H- (N-H stretching 1064 cm^{-1}) and -C-OH (C-OH stretching, 1026 cm^{-1}) for CS and $-COO^-$ (1585 cm^{-1}asymmetric stretching, 1419 cm^{-1}symmetric stretching), -COC-

 doi:10.20944/preprints202409.0850.v1

(C-O-C stretching, 1326 cm^{-1}) and -C-O (C-O stretching, 1060 cm^{-1}) for CMC [30–32]. In the presence of nZVI, displacements are observed in the bands corresponding to the groups -CONH-, -N-H and -C-OH of the CS and $-COO^-$ of CMC, indicating a strong surface anchorage of both CS and CMC on the surface of the nZVI, as reported by other authors [32,33]. The spectrum of CS-NSTAR presented a lower resolution and lower intensity than that of pure CS but the main CS peaks are clearly recognizable and shifted towards lower wave numbers in comparison with the pure CS spectra.

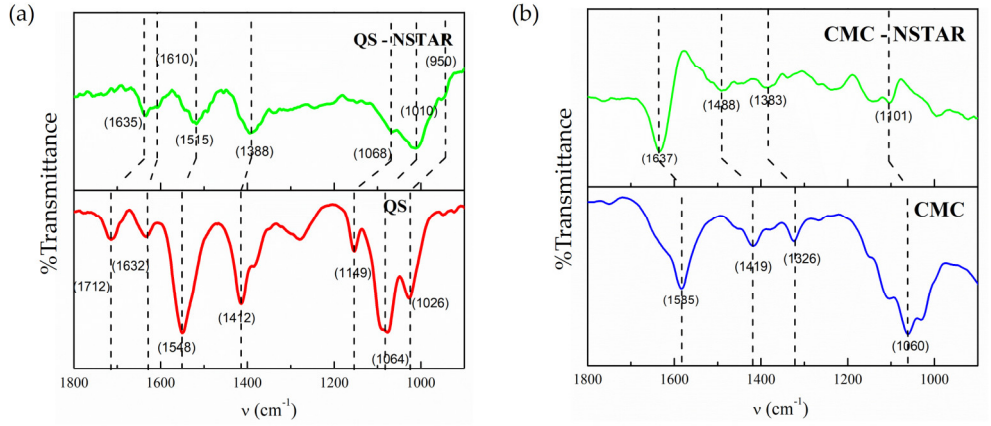

Figure 4. FTIR spectra. (a) CS and CMC in NSTAR film, (b) Pure FTIR spectra of CS and CMC.

The peaks of the triplet between 1000 and 1150 cm^{-1} of the CS spectrum showed shifts of similar magnitude. From the identification of the direction and magnitude of the shifts of these bands it was identified that the bands centered on 1712 cm^{-1}, 1632 cm^{-1}, 1548 cm^{-1} and 1412 cm^{-1} in the pure CS spectrum shifted towards 1635 cm^{-1}, 1610 cm^{-1}, 1515 cm^{-1} and 1388 cm^{-1}, respectively. Shifts were also observed for -CH_2 and -C-O-C groups; however, it is unlikely that these shifts can be attributed to direct interaction between these groups and the nZVI surface due to steric hindrance. Among the bands identified, those that presented the greatest shifts were the ones belonging to the nitrogenous and oxygenated functional groups (1712 cm^{-1}, 1064 cm^{-1} and 1026 cm^{-1}, respectively). The observed shifts would account for an interaction between the groups, -CONH-, -N-H and -C-OH with Fe(II) or Fe(III) on the surface of the nanoparticles [34], for the penta- or hexacoordinate complex of Fe(II).

For the CMC, characteristic bands centered on 1585 cm^{-1}, 1419 cm^{-1}, 1326 cm^{-1}, 1060 cm^{-1} were assigned by identifying them as -COO^- asymmetric, -COO^- symmetrical, -C-O-C- stretch and -C-O stretch, respectively [31]. According to Jones et al., the separation of the symmetrical and asymmetrical sections of the carboxylate groups of CMC determines the type of chelation by which the CMC can be anchored to the metal surface of the Fe. In this case, the distance between the signals describing the presence of symmetrical and asymmetrical carboxylates of CMC was 149 cm^{-1} on the NSTAR film, suggesting that the surface interaction between the NSTAR and the CMC could occur in the form of a bidentate complex [35].

3.2. Removal of Cr(VI)

3.2.1. Removal of Cr(VI) in Synthetic Aqueous Solutions: pH and Immobilization and Type of NCs as Variables

Figure 5 shows the dry-based removal capacity of Cr(VI) as a function of the solution pH when NSTAR@HCS, NSTAR-CMC@HCS and NSTAR-CMC@MCS were used.

 doi:10.20944/preprints202409.0850.v1

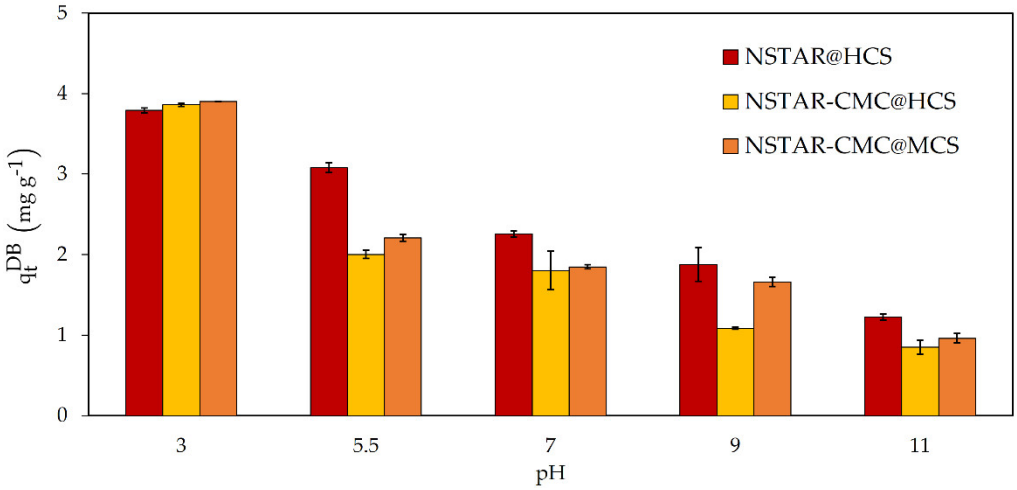

Figure 5. Cr(VI) q_t^{DB} removal capacity with NSTAR-CMC@MCS, NSTAR-CMC@HCS, and NSTAR@HCS. Initial conditions: Synthetic water, $[Cr(VI)]_0$ = 65 μM, 0.7 g NCs, pHs: 5.5, 7, 9 and 11. Total time of the experiment, 2 hours.

In the studied conditions, it was observed that Cr(VI) removal increases with decreasing pH. In experiments performed at pH 3 with the three NCs (results not shown), Cr(VI) removal was higher than at pH 5, consistent with previous results using nZVI in suspension [36]. However, this low pH is problematic because, in acidic media, the beads lose their physical integrity and fracture, during the experiment. Therefore, only pH values of 5.5 or higher were used in the subsequent experiments to ensure the preservation of the bead's structure.

The higher removal of Cr(VI) in acidic conditions when nZVI is used can be explained by analyzing the mechanisms described by equations (1) to (4), that show the reactions of $HCrO_4^-$ or CrO_4^{2-} with Fe(0) and Fe^{2+} result in H^+ consumption. Under acidic conditions, the oxides and hydroxides on the surface of the nZVI dissolve, leaving the Fe(0) in the core exposed and available to reduce Cr(VI). Additionally, H^+ promotes the corrosion of Fe(0) generating Fe^{2+} that consequently reduce Cr(VI) to Cr(III). Under alkaline conditions, however, oxides and hydroxides accumulate on the surface of nZVI, thus reducing the removal efficiency of Cr(VI). It becomes evident that an acidic environment may be preferable for the removal of Cr(VI) in aqueous solution [15,30].

In addition to the aforementioned reactions, it is important to analyze how the distribution of Cr(VI) species, the surface groups of nZVI, and the functional groups of CS and CMC change with pH, considering that the nZVI are immobilized in a CS or CS/CMC matrix.

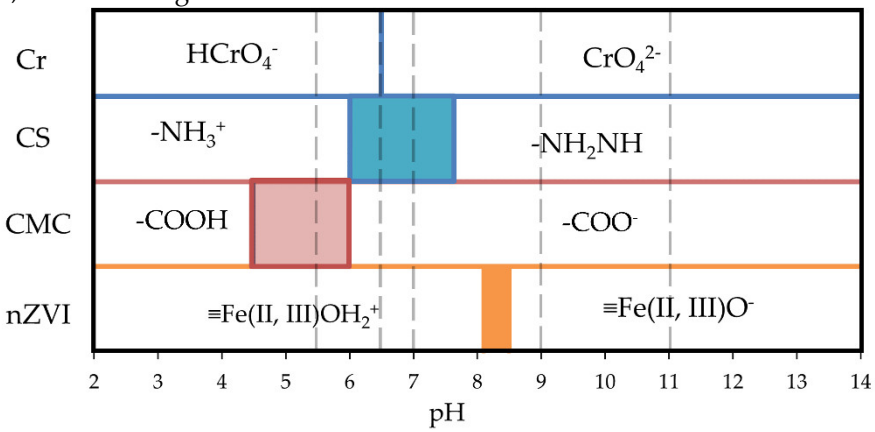

6 outlines the speciation of Cr(VI) in a pH range from 2 to 14 and the distribution of surface species of CS, CMC and nZVI as a function of pH. The scheme was created based on the Pourbaix diagram of chromium [37,38], the pKa of CS [39] and CMC [40], and the isoelectric point of nZVI [41]

 doi:10.20944/preprints202409.0850.v1

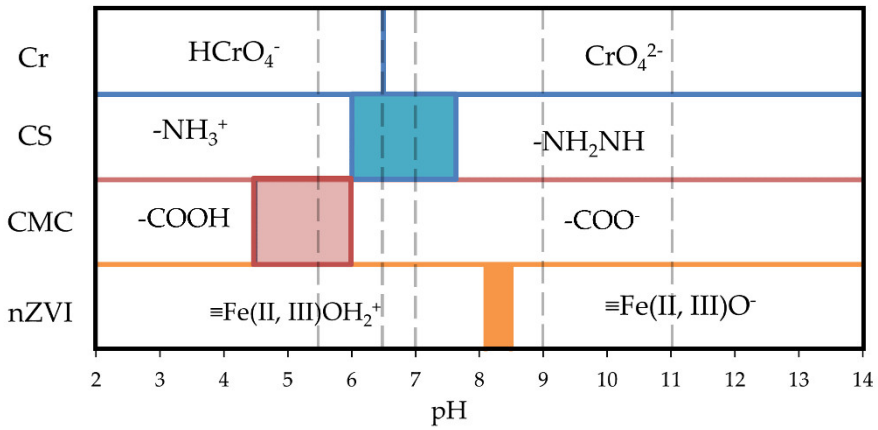

Figure 6. Cr(VI) species distribution and surface species of CS and nZVI as function of pH. The dotted lines correspond to the pH values at which the Cr(VI) removal experiments were performed in this work. The region in blue indicates the range of pKa for the amino groups of CS, the region in red indicates the range of pKa for the carboxyl groups of CMC and the region in green represents the range of values for the nZVI isoelectric points.

In the case of CS, the degree of acetylation is the most influential factor in determining its pKa value, which is widely accepted to be between 6 and 7, with a 95% deprotonation of amines occurring at pH 8 [39]. For CMC, the pKa is a function of the number of –COOH groups per monomer, the degree of dissociation (determined by the pH of the medium) and the ionic strength [40]. The work of Linh et al.[42] was taken as a reference, which reports a pKa of 4.5 reaching total dissociation at pH 6. The adsorption of Cr(VI) on the surface of CS spheres or nZVI will be favored when the chemical species exposed to water of each solid have an opposite charge to that the predominant Cr(VI) ion in solution.

As shown in Figure 6, between pH 2 and 6.5, $HCrO_4^-$ is the predominant Cr(VI) species. If the pH rises above 6.5, the predominant form becomes CrO_4^{2-}. At pH 5.5, Cr is found as the negatively charged $HCrO_4^-$ species, while the surface groups of both CS and nZVI are found as positively charged species with a positive charge ($-NH_3^+$ and $\equiv Fe(II,III)OH_2^+$, respectively), favoring the elimination of Cr(VI) with the NCs. Additionally, at this pH, CMC is neutral, so it is expected that in the Cr(VI) removal experiments performed with NSTAR-CMC@CS, CMC does not influence the removal performance. This type of analysis also explains why an increase in pH is detrimental to the removal efficiency of the NCs. At pH values higher than 6.5, Cr(VI) is found as a negatively charged CrO_4^{2-} species, and the surface groups of CS, CMC, and nZVI are also negatively charged (NH_2-NH, COO^-, and $\equiv Fe(II,III)O^-$, respectively), making the removal of Cr(VI) with the NCs less favorable.

Regarding the removal efficiency comparing the different NCs syntheses, as depicted in Figure 5, NSTAR@HCS demonstrated superior removal efficiency within the studied pH range followed by NSTAR-CMC@MCS and NSTAR-CMC@HCS. Therefore, NSTAR@HCS was selected as the removal material for the experiments performed with the real aqueous sample contaminated with Cr(VI) (Section 3.2.2). **Error! Reference source not found.** compiles Cr(VI) removal efficiencies for different Fe-CS based NCs obtained from bibliography. According to the analysis of the literature presented in Table 2, the removal capacity of Cr(VI) obtained with the NCs synthesized in this work is the highest one but in the order of that found for similar materials based of iron nanoparticles (FeNPs).

Table 2. Cr(VI) removal efficiencies with NCs based on Fe-CS at different pHs obtained from bibliographic analysis.

Ref.	$[Cr(VI)]_0$ (mM)	Material		pH	t (min)	q_t^{DB} (mg Cr(VI) g^{-1}FeNPs)
		NPs	NCs			
This work	0.065	comercial	nZVI@HCS	5.5	120	6.4

 doi:10.20944/preprints202409.0850.v1

				7		4.7
[43]	0.385	comercial	nZVI@CS	6.4	40	1.6
[44]	0.385	comercial	nZVI@CS	3.9	60	4.0
[45]	0.385	comercial	nZVI@CS	3	60	6.0
[46]	0.961	Laboratory synthesized	IONPs@CS	6	480	4.4

IONPs: Iron Oxide Nanoparticles.

Figure 7 compares the Cr(VI) removal capabilities obtained for NSTAR@HCS, HCS spheres, and free NSTARs in suspension at different pH values. It can be observed that Cr(VI) removal capacity with NSTAR@HCS is significantly higher that obtained with only the individual components of the NCs, i.e., HCS spheres or NSTAR in suspension, for all the studied pH conditions. The removal capacity is even higher than the sum of the individual removal capacities. This pattern was also observed when NSTAR-CMC@MCS and NSTAR-CMC@HCS were used and compared to the removal capacities of their individual components (these results are available in the Supporting Information). This enhanced removal capacity observed in the NCs could be attributed to the activation of NSTAR during the synthesis of the NCs. NSTARs have a compact layer of iron oxides on their surface that can hinder the transfer of Fe(0) electrons from their nucleus to the pollutant of interest, in this case Cr(VI). During the acidic dissolution of CS, the NSTAR outer oxide layer would react, and surface defects would appear, resulting in the activation of the nanoparticles, a process that usually requires 48 h of contact with water [47]. This increased Cr(VI) removal capacity of the nZVI after NCs synthesis was also observed in other studies with NCs consisting of non-activated and immobilized nZVI in polymeric matrices such as polyacrylonitrile [48] and alginate [49].

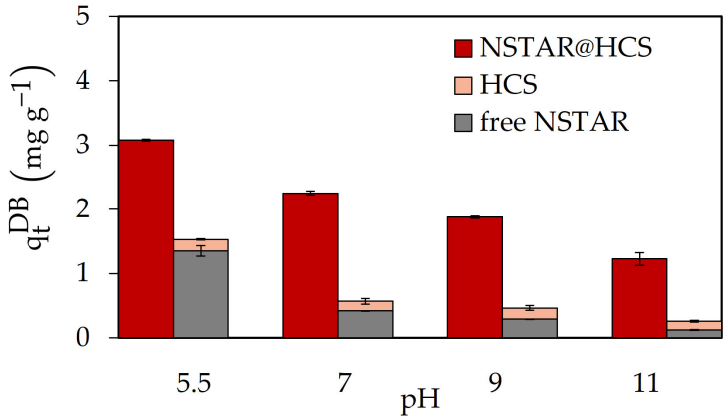

Figure 7. Cr(VI) removal capacity (q_t^{DB}) obtained for NSTAR@HCS, HCS, and free NSTARs in solution. Initial conditions: Synthetic water, $[Cr(VI)]_0$ = 65 μM, 0.7 g NCs, pHs: 5.5, 7, 9 and 11.

It is worth mentioning that the removal capacity of the HCS beads (4.43%, equivalent to 0.373 mg Cr(VI) $g^{-1}_{HCS_{DB}}$) is similar to that reported in the literature for polymeric CS matrices (Liu, 2010, T. Liu, 2012). Taking into account that 97% of the NCs are, after 24 h of reaction, the total amount of Cr(VI) retained inside the beads volume corresponds to Cr(VI) dissolved in water contained inside the NCs. Regarding the removal across different NC syntheses, as depicted in Figure 4, NSTAR@HCS demonstrated superior removal efficiency within the studied pH range. Therefore, it was also selected as the removal material for experiments with real Cr(VI) contaminated water.

3.2.2. Cr(VI) Removal in Real Water: Kinetics

Cr(VI) removal experiments were performed adding NSTAR@HCS to the laboratory effluent. Table 4 shows parameters obtained according to each kinetic adjustment applied: Langmuir pseudo-first, pseudo-second order and intraparticle diffusion kinetic models. Kinetic fit curves are displayed along with support information.

 doi:10.20944/preprints202409.0850.v1

Table 4. Kinetic adjustments using the Langmuir models for pseudo first and second order and the intraparticle diffusion model.

Model		Experiment (m NCs)				
		1 g	2 g	3 g	4 g	6 g
Pseudo 1st order	k_1 (min^{-1})	0.08	0.04	0.08	0.06	0.05
	q_e^{WB} (mg g^{-1})	0.18	0.19	0.18	0.22	0.18
	R^2	0.96	0.95	0.89	0.93	0.91
Pseudo 2nd order	k_2 (g min^{-1}mg^{-1})	0.34 ± 0.12				
	q_e^{WB} (mg g^{-1})	0.21	0.21	0.21	0.24	0.20
	R^2	0.95	0.97	0.95	0.97	0.96
Intraparticular diffusion	k (mg g^{-1} min$^{1/2}$)	0.02	0.02	0.02	0.02	0.02
	R^2	0.69	0.93	0.79	0.87	0.88

According to Table 4, both pseudo-first and pseudo-second-order models provide good fits, with the pseudo-second-order model showing the best fit, an average R^2 of 0.96 ± 0.01. In contrast, adjustments made using the intraparticle diffusion model showed poor fits, with R^2 values ranging from 0.69 to 0.92.

After obtaining the corresponding k_2 for each NCs mass an averaged k_2 was calculated and fixed as fitting parameter, leading to the R^2 and q_e^{WB} values in Table 4. The kinetic constant obtained is of greater magnitude compared to that obtained with similar materials (Zhang, 2018; Wang, 2023). It is worth mentioning that the removal capacity was similar for all the NC masses tested (q_e^{DB}= 0.22 ± 0.02 mg Cr(VI) $g^{-1}_{NC_{WB}}$), which implies that the NCs reached their maximum removal capacity, achieving saturation with each mass. The dry-based Cr(VI) removal capacity (q_e^{DB}) for real water was slightly higher than that obtained in synthetic waters (7.2 vs. 6.4 mg Cr(VI) $g^{-1}_{NC_{DB}}$), which can be attributed to the higher ionic strength present in real waters. This higher ionic strength accelerates the corrosive process of Fe in the NCs, which governs the removal of Cr(VI) [50,51].

As observed in Table 5, the pseudo-second-order kinetic constants reported in literature are lower than those obtained in this study. Wang et al. [54] and Xu et al. [55], using materials like those used here, reported kinetic constants between 10 and 100 times lower, which gives us the guideline that the removal system obtained is kinetically faster than that obtained by other authors, a vehement when it comes to removing Cr(VI).

Table 5. Kinetic constants reported for Cr(VI) removal in similar systems.

Ref.	Material	Pollutant	Constants Adjustment pseudo 2nd order (g min^{-1}mg^{-1})	R^2
This work	nZVI@CS	Cr(VI)	0.34	0.96
[52]	nZVI-BC	Cr(VI)	0.44 2.93	0.88 0.91
[53]	$NiFe_2O_4$-CS	Cr(VI)	3.2×10^{-2}	0.98
[54]	CS-nZVI@BC-hydrogel	Cr(VI)	3.1×10^{-3} 2.8×10^{-3} 2.1×10^{-3}	0.99
[55]	BC stabilized with nZVI supported in CS	Cr(VI)	2.5×10^{-2}	0.99

BC: Biochar.

3.2.3. Chromium Removal Capacity in Real Water

Figure 8 (a) shows the percentage of Cr(TOTAL) removed (%RCr(TOTAL)) for the experiments undertaken with the Cr(VI) contaminated laboratory effluent as a function of the mass of NSTAR@HCS used after 24 h of experiment. Cr(VI) and Cr(TOTAL) concentrations found in solution

 doi:10.20944/preprints202409.0850.v1

were similar for all the NCs masses studied, indicating that no Cr(III) was left in solution after contact with the NCs (see in the Supporting information).

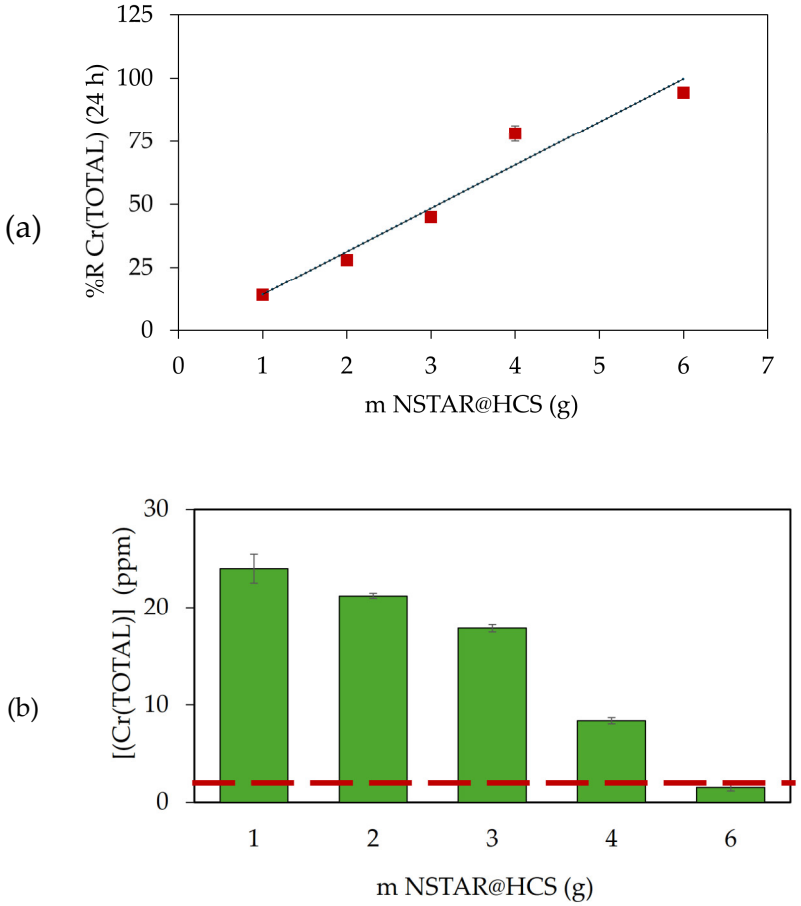

Figure 8. (a) %RCr(TOTAL) for experiments undertaken with Cr(VI) contaminated laboratory effluent as a function of the mass of NSTAR@HCS used in each experiment at 24 h. (b) Cr(TOTAL) concentrations obtained after 24 h for different masses of NSTAR@HCS. Red dotted line: limit of Cr(TOTAL) established by ACUMAR for the discharge of liquid effluents.

As can be seen, the percentage of chromium removal increased in direct proportion to the mass of NSTAR@HCS added for each experiment, achieving almost complete removal with 6 g of NSTAR@HCS.

As shown in Figure 8 (b), using 6 g of NCs to treat 50 mL of chromium-contaminated real water samples successfully meets the discharge limit for total chromium (Cr(TOTAL) ≤ 2 mg L^{-1}) set by ACUMAR [11]. These results demonstrate the promising potential of this technology for chromium removal from water.

3.2.4. Variation of Carbon Content after Treatment

The variation of total carbon (TC), total organic carbon (TOC), and inorganic carbon (IC) post-removal of Cr(VI) was evaluated as a function of the NSTAR@HCS mass used. Figure 11 shows that increasing the amount of NSTAR@HCS results in higher values for these parameters, with TC ranging from 3 to 9 mg L^{-1}. Although these values are of the same order of magnitude as the TC of the effluent, measured at 3.77 ppm, this suggests a correlation between the amount of chitosan released into the solution and the NSTAR@HCS mass used.

 doi:10.20944/preprints202409.0850.v1

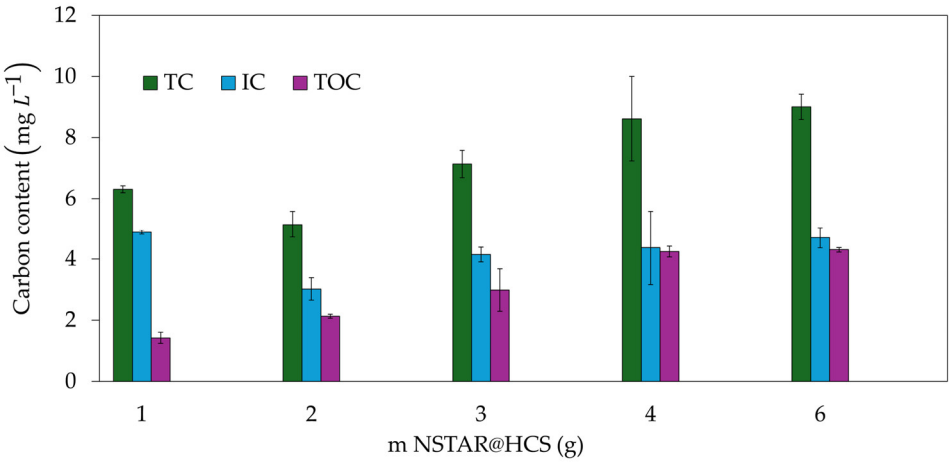

Figure 11. TC, IC and TOC concentrations post Cr(VI) removal in real waters obtained after 24 h for different masses of NSTAR@HCS.

The maximum TOC value obtained in the Cr(VI) removal experiments for the measured samples was 4.8 mg L^{-1} when using 6 g of NCs. Considering that typical COD/TOC ratios for the chemical industry range from 2.5 to 3.5 [56], we can estimate the maximum COD for these samples to be between 10.9 and 15.3 mg L^{-1}, which is well below the discharge limits set by ACUMAR. According to ACUMAR regulations, the allowable COD discharge limit in liquid effluents is ≤ 700 mg L^{-1}.

3.2.5. Cost Analysis and Feasibility of NSTAR@HCS for Cr(VI) Effluent Treatment

Based on the results from this work and considering that the INTI laboratory produces 30 L of this effluent annually, it is estimated that 3.6 Kg of wet NCs would be required to treat the entire annual volume. This amount of NCs corresponds to 108 g of dry-based NSTAR@HCS, comprising 43.1 g of nZVI and 64.9 g of HCS. Given this required amount, an cost analysis was conducted and the details provided in Table 6. For the analysis, the cost considered included those of the main reactants used in the NCs synthesis, the energy associated with operating the equipment (detailed in the supporting information), and the labor costs for producing the required mass of NCs during a standard 8-hour workday.

Table 6. Costs associated with the treatment of the annual volume of a Cr(VI) contaminated laboratory effluent (30 L).

Treatment with NCs	Mass of material (g)	Cost per unit mass (USD/ kg)	Total cost (USD)
NSTAR (NANOIRON)	43.2	430	18.6
HCS (GIHON)	64.8	196	12.7
Electricity cost	1.35 USD/ h		10.8
Synthesis cost (man-hours)	3.75 USD/ h		30
NSTAR@HCS	TOTAL		72.1

The total cost was calculated to be 71.2 USD, which is approximately three times lower than the quoted cost of USD 319 provided by an effluent treatment company that offers waste transfer and treatment services to laboratories in Argentina as of December 2023. This indicates a significant economic advantage of using our material compared to outsourcing the treatment of effluents. Additionally, the simplicity of our method and the fact that chemistry lab personnel possess the necessary knowledge to manage the treatment further enhance its practicality and cost-effectiveness.

4. Conclusions

 doi:10.20944/preprints202409.0850.v1

The NCs produced, consisting of NSTAR immobilized in chitosan (CS), exhibited a stable structure and high efficiency in removing Cr(VI) from water. Various synthesis routes were explored, including the pre-stabilization of the nanoparticles with CMC and the use of MCS and HCS. Comprehensive characterization of the materials was performed using SEM-EDS, XRD, FTIR and DMA. It was found that NCs formed millimeter-sized spheres with micrometer-sized aggregates of randomly distributed nZVI, and the α-Fe phase of nZVI was partially preserved after synthesis, predominating, especially in the NCs synthesized from CMC-MCS and HCS.

It was also determined that CS binds to Fe(II) or Fe(III) on the surface of nZVI through its -C-OH, -N-H and -CONH- functional groups, analogous to the Fe(II)-CS complex in solution. Additionally, CMC binds to surface Fe species through the COO- functional group, forming a bidentate bridge complex. According to DMA, the NCs with the highest mechanical resistance were NSTAR@HCS, which were later used for the removal of Cr(VI) in real water samples.

The NCs proved to be highly efficient in removing Cr(VI), particularly in acidic environments, as expected. When tested on real effluents, the NCs were effectively complied with both national and international regulation for Cr(TOTAL) limits and national regulations for TOC levels. Additionally, they demonstrate a competitive cost when compared to outsourcing effluent treatment. These materials show promising potential for environmental remediation applications, both in synthetic waters and laboratory wastewater containing Cr(VI).

6. Patents

This section is not mandatory but may be added if there are patents resulting from the work reported in this manuscript.

Supplementary Materials: The following supporting information can be downloaded at the website of this paper posted on Preprints.org, Table S1: Main characteristics of the commercial nZVI (NSTAR) used in the synthesis of NCs; Dynamic Mechanical Analysis detailed procedure and fundamentals (includes Figures S1. Experimental arrangement used for DMA and S2. Stress*-strain obtained from the DMA for NSTAR@HCS, NSTAR-CMC@MCS, HCS, and NSTAR-CMC@HCS); Figure S3. Cr(VI) removal capabilities obtained for NSTAR-CMC@HCS, CMC@HCS, and free NSTARs in solution. Initial conditions: Synthetic water, $[Cr(VI)]_0 = 65$ μM, 0.7 g NCs, pHs: 3, 5.5, 7, 9 and 11; Figure S4. Cr(VI) removal capabilities obtained for NSTAR-CMC@MCS, CMC@MCS, and free NSTARs in solution. Initial conditions: Synthetic water, $[Cr(VI)]_0 = 65$ μM, 0.7 g NCs, pHs: 3, 5.5, 7, 9 and 11; Table S2. Cr(VI) and Cr(TOTAL) concentrations obtained after 24 h for different masses of NSTAR@HCS; Table S3. Costs associated with the electricity consumption required to produce NCs based on nZVI and CS.

Author Contributions: Conceptualization: V.N.M and N.Q.; methodology, V.N.M. and N.Q.; formal analysis, I.D.R., U.C., V.N.M. and N.Q; investigation, I.D.R. and V.N.M.; data curation, I.D.R., U.C. and V.N.M.; writing—original draft preparation, I.D.R. and V.N.M; writing—review, V.N.M. and N.Q; editing, N.Q.; project administration, V.N.M. and N.Q.; funding acquisition, V.N.M. and N.Q. All authors have read and agreed to the published version of the manuscript.

Funding: This work was supported by Agencia Nacional de Promoción Científica y Tecnológica (ANPCyT, Argentina) PICT Projects 2018-3114 and 2018-1296, by Universidad Tecnológica Nacional, PID Project MSECABA0008452TC and Consejo Nacional de Investigaciones Científicas y Técnicas (CONICET) PIP Project 11220200101024CO.

Data Availability Statement: The data presented in this study are available in the article and the supplementary material.

Acknowledgments: The authors thank their corresponding institutions for their financial support.

Conflicts of Interest: The authors declare no conflicts of interest. The funders had no role in the design of the study; in the collection, analyses, or interpretation of data; in the writing of the manuscript; or in the decision to publish the results.

References

1. De Souza Nascimento, E., Filho, A.T.: Chemical waste risk reduction and environmental impact generated by laboratory activities in research and teaching institutions, Brazilian Journal of Pharmaceutical Sciences vol. 46, n. 2, abr./jun., 2010. https://doi.org/10.1590/S1984-82502010000200004
2. Osiska, R. M.; Benitez, M. E.; Gimenez, M. C.: Gestión y manejo de residuos químicos en el laboratorio: una manera de prevenir la contaminación del medio ambiente. Universidad Nacional del Nordeste. Reunión de Comunicaciones Científicas y Tecnológicas, 2004.
3. Antoniassi, B., Araujo, V., Chaves, M., Telascrea, M., Kempa, M., Bersanetti, B.: Analysis of the Economic Viability in the Implementation of the Chemical Waste Management System in Teaching and Research Laboratories. J Sustain Dev. 10, 112, 2017. https://doi.org/10.5539/jsd.v10n1p112
4. Gao, Y., Yang, X., Lu, X., Li, M., Wang, L., Wang, Y.: Kinetics and Mechanisms of Cr(VI) Removal by nZVI: Influencing Parameters and Modification. Catalysts. 12, 2022. https://doi.org/10.3390/catal12090999
5. Liu, A., Liu, J., Han, J., Zhang, W.X.: Evolution of nanoscale zero-valent iron (nZVI) in water: Microscopic and spectroscopic evidence on the formation of nano- and micro-structured iron oxides. J Hazard Mater. 322, 129–135, 2017. https://doi.org/10.1016/j.jhazmat.2015.12.070
6. Quici, N., Meichtry, M., Montesinos, V.N.: Use of Nanoparticulated Iron Materials for Chromium, Arsenic, and Uranium Removal from Water. In: Marta I, L., Quici, N., and Meichtry, J.M. (eds.) Iron Nanomaterials for Water and Soil Treatment. pp. 177–188. Pan Stanford Publishing, 2018.
7. Barka, E., Noutsopoulos, C., Galani, A., Panagou, I., Kalli, M., Koumaki, E., Malamis, S., Mamais, D.: Removal of Contaminants of Emerging Concern from Wastewater Using an Integrated Column System Containing Zero Valent Iron Nanoparticles. Water (Switzerland). 15, 2023. https://doi.org/10.3390/w15030598
8. Li, S., Wang, W., Liang, F., Zhang, W.: Heavy metal removal using nanoscale zero-valent iron (nZVI): Theory and application. J Hazard Mater. 322, 1–9, 2016. https://doi.org/10.1016/j.jhazmat.2016.01.032
9. Crane, R.A., Scott, T.B.: Nanoscale zero-valent iron: Future prospects for an emerging water treatment technology. J Hazard Mater. 211–212, 112–125, 2012. https://doi.org/10.1016/j.jhazmat.2011.11.073
10. Liu, J., Sun, S., Zhang, H., Kong, Q., Li, Q., Yao, X.: Remediation materials for the immobilization of hexavalent chromium in contaminated soil: Preparation, applications, and mechanisms, Environmental Research 237, 116918, 2023. https://doi.org/10.1016/j.envres.2023.116918
11. ACUMAR: Anexos Resolución E 46/2017, http://servicios.infoleg.gob.ar/infolegInternet/anexos/270000-274999/273042/res46.pdf
12. Raji, M., Mirbagheri, S.A., Ye, F., Dutta, J.: Nano zero-valent iron on activated carbon cloth support as Fenton-like catalyst for efficient color and COD removal from melanoidin wastewater. Chemosphere. 263, 2021. https://doi.org/10.1016/j.chemosphere.2020.127945
13. Ibrahim, H.M., Awad, M., Al-farraj, A.S., Al-turki, A.M.: Stability and dynamic aggregation of bare and stabilized zero-valent iron nanoparticles under variable solution chemistry. Nanomaterials. 10, 2020. https://doi.org/10.3390/nano10020192
14. Subedi, N., Lähde, A., Abu-Danso, E., Iqbal, J., Bhatnagar, A.: A comparative study of magnetic chitosan (Chi@Fe3O4) and graphene oxide modified magnetic chitosan (Chi@Fe3O4GO) nanocomposites for efficient removal of Cr(VI) from water. Int J Biol Macromol. 137, 948–959, 2019. https://doi.org/10.1016/j.ijbiomac.2019.06.151
15. Wang, J., Zhuang, S.: Removal of various pollutants from water and wastewater by modified chitosan adsorbents. Crit Rev Environ Sci Technol. 47, 2331–2386, 2017. https://doi.org/10.1080/10643389.2017.1421845
16. Ahmadi, M., Foladivanda, M., Jaafarzadeh, N., Ramezani, Z., Ramavandi, B., Jorfi, S., Kakavandi, B.: Synthesis of chitosan zero-valent iron nanoparticles-supported for cadmium removal: characterization, optimization and modeling approach. Journal of Water Supply: Research and Technology - Aqua. 66, 116–130, 2017. https://doi.org/10.2166/aqua.2017.027
17. Sabu Thomas: Advances in Natural Polymers. Springer Berlin Heidelberg, Berlin, Heidelberg, 2013.
18. Cumbal, L., Zuñiga, M.: Chitosan dispersed with Fe(III) oxide particles: A sorbent used for selective removal of arsenic from contaminated waters. In *Book Title*: The Global Arsenic Problem, 2010. DOI: 10.1201/b10537-19
19. Weisz, A.D., Rodenas, L.G., Morando, P.J., Regazzoni, A.E., Blesa, M.A.: FTIR study of the adsorption of single pollutants and mixtures of pollutants onto titanium dioxide in water: oxalic and salicylic acids. Catalysis Today 76, 103–112, 2002. https://doi.org/10.1016/S0920-5861(02)00210-9
20. Eckert, J.M., Judd, R.J., Lay, P.A.: Response of chromium(V) to the diphenylcarbazide spectrophotometric method for the determination of chromium(VI). Analytica Chimica Acta, Volume 255, 31-33, 1991. https://doi.org/10.1016/0003-2670(91)85083-5.
21. Liu, J.F., Zhao, Z.S., Jiang, G.B.: Coating Fe_3O_4 magnetic nanoparticles with humic acid for high efficient removal of heavy metals in water. Environ Sci Technol. 42, 6949–6954, 2008. https://doi.org/10.1021/es800924c

22. Schwertmann, U., Carlson, L.: Iron Oxides in the Laboratory: Preparation and Characterization. 2nd Ed. John Wiley & Sons, 2000. pp. 125-147, 2000. ISBN 3527296697, 9783527296699.
23. Kumar, S., Koh, J.: Physiochemical, optical and biological activity of chitosan-chromone derivative for biomedical applications. Int J Mol Sci. 13, 6102–6116, 2012. https://doi.org/10.3390/ijms13056102
24. Coreño-Alonso, J., Teresa Méndez-Bautista, M.: Relación estructura-propiedades de polímeros. Educ. quím., 21(4), 291-299, 2010. Universidad Nacional Autónoma de México, ISSN 0187-893-X. Publicado en línea el 10 de septiembre de 2010, ISSNE 1870-8404.
25. Morello, G., Quarta, A., Gaballo, A., Moroni, L., Gigli, G., Polini, A., Gervaso, F.: A thermo-sensitive chitosan/pectin hydrogel for long-term tumor spheroid culture. Carbohydr Polym. 274, 2021. https://doi.org/10.1016/j.carbpol.2021.118633
26. Morello, G., Polini, A., Scalera, F., Rizzo, R., Gigli, G., Gervaso, F.: Preparation and characterization of salt-mediated injectable thermosensitive chitosan/pectin hydrogels for cell embedding and culturing. Polymers (Basel). 13, 2021. https://doi.org/10.3390/polym13162674
27. Wang, T., Jin, X., Chen, Z., Megharaj, M., Naidu, R.: Simultaneous removal of Pb(II) and Cr(III) by magnetite nanoparticles using various synthesis conditions. Journal of Industrial and Engineering Chemistry. 20, 3543–3549, 2014. https://doi.org/10.1016/j.jiec.2013.12.047
28. Liu, T., Sun, Y., Wang, Z.L.: Stabilized chitosan/Fe0-nanoparticle beads to remove heavy metals from polluted sediments. Water Science and Technology. 73, 1090–1097, 2016. https://doi.org/10.2166/wst.2015.556
29. Dima, J.B., Sequeiros, C., Zaritzky, N.E.: Hexavalent chromium removal in contaminated water using reticulated chitosan micro/nanoparticles from seafood processing wastes. Chemosphere. 141, 100–111, 2015. https://doi.org/10.1016/j.chemosphere.2015.06.030
30. Horzum, N., Demir, M.M., Nairat, M., Shahwan, T.: Chitosan fiber-supported zero-valent iron nanoparticles as a novel sorbent for sequestration of inorganic arsenic. RSC Adv. 3, 782, 2013. https://doi.org/10.1039/c3ra23454a
31. He, F., Zhao, D., Liu, J., Roberts, C.B.: Stabilization of Fe-Pd Nanoparticles with Sodium Carboxymethyl Cellulose for Enhanced Transport and Dechlorination of Trichloroethylene in Soil and Groundwater. 5, 70–72, 2007. https://doi.org/10.1364/OL.5.000070
32. Socrates, G.: Infrared and Raman Characteristic Group Frequencies Contents. 3rd Ed. JOHN WILEY & SONS, LTD. 2001, ISBN 0 470 09307 2.
33. Zia, K.M., Zuber, M., Bhatti, I.A., Barikani, M., Sheikh, M.A.: Evaluation of biocompatibility and mechanical behavior of polyurethane elastomers based on chitin/ 1,4-butane diol blends. Int. J. Biolog. Macromol. 44, 18–22, 2009. https://doi.org/10.1016/j.ijbiomac.2008.09.011
34. Bhatia, S.C., Ravi, N.: A magnetic study of an Fe-chitosan complex and its relevance to other biomolecules. Biomacromolecules. 1, 413–417, 2000. https://doi.org/10.1021/bm0002959
35. Jones, F., Rohl, A.L., Farrow, J.B., van Bronswijk, W.: Molecular modeling of water adsorption on hematite. Physical Chemistry Chemical Physics. 2, 3209–3216, 2000. https://doi.org/10.1039/b003380o
36. Montesinos, V.N., Quici, N., Litter, M.I.: Visible light enhanced Cr(VI) removal from aqueous solution by nanoparticulated zerovalent iron. Catal. Commun. 46, 57–60, 2014. https://doi.org/http://dx.doi.org/10.1016/j.catcom.2013.11.024
37. Mohan, D., Pittman, C.U.: Activated carbons and low cost adsorbents for remediation of tri- and hexavalent chromium from water, 2006. doi: 10.1016/j.jhazmat.2006.06.060
38. Takeno, N.: Atlas of Eh-pH diagrams Intercomparison of thermodynamic databases, Tsukuba. 2005. ISBN 978-0915567980
39. Xu, P., Bajaj, G., Shugg, T., Van Alstine, W.G., Yeo, Y.: Zwitterionic chitosan derivatives for pH-sensitive stealth coating. Biomacromolecules. 11, 2352–2358, 2010. https://doi.org/10.1021/bm100481r
40. Metodiev, A.: Electric Properties of Carboxymethyl Cellulose. Chapter 8 in: Cellulose - Fundamental Aspects. InTech, 2013. http://dx.doi.org/10.5772/56935
41. Sun, Y.P., Li, X., Cao, J., Zhang, W., H. Paul Wang.: Characterization of zero-valent iron nanoparticles. Adv Colloid Interface Sci. 120, 47–56–47–56, 2006. https://doi.org/10.1016/j.cis.2006.03.001
42. Cuba-Chiem, L. T., Huynh, L., Ralston, J. and Beattie, D. A.: In Situ Particle Film ATR FTIR Spectroscopy of Carboxymethyl Cellulose Adsorption on Talc: Binding Mechanism, pH Effects, and Adsorption Kinetics. Langmuir. 24, 8036–8044, 2008. https://doi.org/10.1021/la800490t
43. Liu, T., Zhao, L., Sun, D., Tan, X.: Entrapment of nanoscale zero-valent iron in chitosan beads for hexavalent chromium removal from wastewater. J Hazard Mater. 184, 724–730, 2010. https://doi.org/10.1016/j.jhazmat.2010.08.099
44. Liu, T.Y., Zhao, L., Wang, Z.L.: Removal of hexavalent chromium from wastewater by Fe0-nanoparticles-chitosan composite beads: characterization, kinetics and thermodynamics. Water Sci Technol. 66, 1044–1051, 2012. https://doi.org/10.2166/wst.2012.278

 doi:10.20944/preprints202409.0850.v1

45. Liu, T., Wang, Z.-L., Zhao, L., Yang, X.: Enhanced chitosan/Fe0-nanoparticles beads for hexavalent chromium removal from wastewater. Chemical Engineering Journal. 189–190, 196–202, 2012. https://doi.org/10.1016/j.cej.2012.02.056
46. Jawed, A., Golder, A.K., Pandey, L.M.: Bio-based iron oxide nanoparticles forming bi-functional chitosan composite adsorbent for Cr(VI) decontamination. Chemical Engineering Journal. 481, 2024. https://doi.org/10.1016/j.cej.2023.148411
47. NANOIRON. Manual for preparation of an aqueous dispersion from NSTAR powder, 2024. https://nanoiron.cz/en/products/zero-valent-iron-nanoparticles/nanofer-star
48. Sciscenko, I., Luca, V., Ramos, C.P., Scott, T.B., Montesinos, V.N., Quici, N.: Immobilization of nanoscale zerovalent iron in hierarchically channelled polyacrylonitrile for Cr(VI) remediation in wastewater. Journal of Water Process Engineering. 39, 2021. https://doi.org/10.1016/j.jwpe.2020.101704
49. Parnis, M., García, F.E., Toledo, M.V., Montesinos, V.N., Quici, N.: Zerovalent Iron Nanoparticles-Alginate Nanocomposites for Cr(VI) Removal in Water—Influence of Temperature, pH, Dissolved Oxygen, Matrix, and nZVI Surface Composition. Water (Switzerland). 14, 2022. https://doi.org/10.3390/w14030484
50. Reinsch, B.C., Forsberg, B., Penn, R.L., Kim, C.S., Lowry, G. V.: Chemical transformations during aging of zerovalent iron nanoparticles in the presence of common groundwater dissolved constituents. Environ Sci Technol. 44, 3455–3461, 2010. https://doi.org/10.1021/es902924h
51. Bae, S., Collins, R., Waite, T., Hanna, K.: Advances in Surface Passivation of Nanoscale Zerova-lent Iron A. Critical Review. Environmental Science and Technology. 52, 12010–12025, 2018. https://doi.org/10.1021/acs.est.8b01734ï
52. Chen, X.L., Li, F., Xie, X.J., Li, Z., Chen, L.: Nanoscale zero-valent iron and chitosan functionalized eichhornia crassipes biochar for efficient hexavalent chromium removal. Int J Environ Res Public Health. 16, 2019. https://doi.org/10.3390/ijerph16173046
53. Zhang, B., Wu, Y., Fan, Y.: Synthesis of Novel Magnetic NiFe2O4 Nanocomposite Grafted Chitosan and the Adsorption Mechanism of Cr(VI). J Inorg Organomet Polym Mater. 29, 290–301, 2019. https://doi.org/10.1007/s10904-018-0987-4
54. Wang, T., Sun, Y., Bai, L., Han, C., Sun, X.: Ultrafast removal of Cr(VI) by chitosan coated biochar-supported nano zero-valent iron aerogel from aqueous solution: Application performance and reaction mechanism. Sep Purif Technol. 306, 2023. https://doi.org/10.1016/j.seppur.2022.122631
55. Xu, H., Gao, M., Hu, X., Chen, Y., Li, Y., Xu, X., Zhang, R., Yang, X., Tang, C., Hu, X.: A novel preparation of S-nZVI and its high efficient removal of Cr(VI) in aqueous solution. J Hazard Mater. 416, 2021. https://doi.org/10.1016/j.jhazmat.2021.125924
56. Wojnárovits, L., Homlok, R., Kovács, K., Tegze, A., Takács, E.: Wastewater Characterization: Chemical Oxygen Demand or Total Organic Carbon Content Measurement? Molecules. 29, 2024. https://doi.org/10.3390/molecules29020405
57. Sheydvasser, A.: 3.1 Steiner's porism and 3.6 Steiner's porism revisited, Linear Fractional Transformations, Undergraduate Texts in Mathematics, Springer International Publishing, pp. 75–81, 99–101, 2023. doi:10.1007/978-3-031-25002-6, ISBN 978-3-031-25001-9, S2CID 258177153)